

LANGLEY FACILITY FOR TESTS AT MACH 7 OF SUBSCALE, HYDROGEN-BURNING,

AIRFRAME-INTEGRATABLE, SCRAMJET MODELS

William B. Boatright,* Alexander P. Sabol,** Daniel I. Sebacher,**
 Shimer Z. Pinckney,** and Robert W. Guy**
 NASA Langley Research Center
 Hampton, Virginia 23665

Abstract

Modifications to a 20-megawatt arc-heated facility for testing a hydrogen-burning, airframe-integratable, subscale, scramjet model are described. Arc-heated flow is mixed with unheated air to furnish a test flow duplicating Mach 7 flight. (Stagnation temperature is 2220° K.) Modifications to the commercially available heater to improve survivability and smoothness are described. Pitot profiles show uniform flow and a slightly thinner nozzle boundary layer than predicted. Comparison of the tunnel boundary layer, which will be ingested by the engine model, with the boundary layer that a flight engine might ingest from its vehicle forebody shows a difference in the density distribution through the boundary layer. Calculations of wall heating and transient wall temperatures of the engine model show that for a 30-sec burn, the heat sink model requires cooling at selected locations to avoid thermal-stress, cycle-life problems. Model performance predictions show that fuel equivalence ratio and nozzle exit area both have large effects on thrust. Average inlet entrance Mach number (as affected by boundary-layer ingestion) has little effect on thrust.

Symbols

$A_0, A_1, A_{\text{cowl}}$	Cross-sectional areas on engine model, see Figure 15
A_2, A_3, A_4	
h_c	Capture height
M	Mach number
P_T	Stagnation pressure
P_{T2}	Stagnation pressure behind a normal shock
P_1	Static pressure
q	Dynamic pressure
Re_θ	Reynolds number based on boundary-layer momentum thickness
T_T	Stagnation temperature
U	Velocity
x	Longitudinal distance
y	Vertical distance

* Head, Performance Section, High-Speed Aerodynamics Division. Associate Fellow, AIAA.

** Aerospace Technologist, High-Speed Aerodynamics Division.

β	Flow angle of nozzle exhaust from engine
δ^*	Boundary-layer displacement thickness
η_c	Combustion efficiency
ρ	Density
ϕ	Fuel equivalence ratio (a value of unity for stoichiometric combustion)

Subscripts

a	Air
f	Fuel
∞	Free stream

Introduction

The hydrogen-fueled scramjet engine, when integrated into an aircraft design, promises significant advances in performance, efficiency, and payload capability for future aircraft. Applications exist in space, military, and commercial fields. The design concept which uses the aircraft fuselage to process the air entering and leaving the engine, Figure 1, tends to maximize thrust per square foot of capture area with low external drag. Figure 1 shows an integrated engine-airframe design concept in the upper part of the figure. Modularization of the engine will ease ground test facility requirements and results of several analyses¹⁻⁴ show this design concept offers advantages in many important ways.

At NASA Langley Research Center there is a research effort directed toward developing the technology for a fixed-geometry, hydrogen-burning, scramjet engine module suitable for the integrated engine-airframe configuration. In addition to basic fluid mechanic and combustion research,⁵ engine component research,^{6,7} and structural research,⁸ subscale aerothermal tests of the scramjet configuration are needed as an economical and expeditious approach to evaluate interactions between components, to refine the engine design, and to provide convincing performance data.

The subscale engine testing requires a facility which provides duplication of the temperature or energy content of the air as well as Mach number and altitude, and the test section must be sufficiently large to accommodate an engine model large enough for meaningful design detail (so that fuel injection geometry, combustion, and mixing lengths will have meaning in terms of practical sized engines). The facilities which exist in the United States with

this capability are relatively few. For example, the Air Force Airbreathing Propulsion Test Unit (APTU) at Arnold Engineering Development Center, Tullahoma, Tenn., the Marquardt Test Cell No. 8 at Van Nuys, Calif., and the NASA Hypersonic Propulsion Facility at the Plumbrook Station of Lewis Research Center (closed June 1974) provide the size and high-temperature air capability, but testing in these research facilities is expensive for the kind of small-scale, research-oriented, configuration development needed in the early stages of the engine technology development program. Other smaller facilities such as those located at General Applied Science Laboratories, Westbury, New York, and the Applied Physics Laboratory, Silver Spring, Maryland, are also capable of adaptation to subscale, engine module testing of the integratable configuration. To supply the facility need for the subscale research-oriented engine tests, an existing electric-arc-heated facility at Langley has been modified with design specifications required for the subscale engine tests of an integratable scramjet configuration under conditions duplicating Mach 7 flight. These tests are envisioned as only aerothermodynamic in purpose (not regeneratively cooled structures) and will use models designed as simply as possible. The models, using largely heat-sink materials, will permit economical configuration changes necessary for finalization of the engine internal contours and fuel injection schemes before fabrication of an engine with a more expensive flight-weight structure. The NASA Hypersonic Research Engine Project⁹ significantly advanced fabrication technology and much of this technology will be applicable to the structural design of the final engine configuration when the aerothermal technology of the integratable configuration is more firmly established.

This report documents the considerations and analyses that influenced the design of the modified facility, presents preliminary data obtained on flow calibration and arc-heater performance, discusses some of the operating problems encountered, and describes model design, instrumentation, and predicted scramjet performance.

Simulation Capability

Tunnel Power-Size Considerations

In order to make tests duplicating Mach 7 flight, the stagnation temperature of the air must be 2220° K (4000° R). Electric-arc-heating furnishes more than adequate air temperatures, but the problem with their use consists of furnishing sufficient power to the tunnel airstream to provide a facility with adequate size and low enough altitude simulation. Figure 2 shows power in the airstream as a function of throat area. The power supply for this facility has a 20-megawatt capacity but considering arc-heater efficiency and the need for ballast resistance in the circuit, the power actually put into the air is in the 5- to 7-megawatt range. The 0.272- by 0.305-meter (10.7- by 12-in.) nozzle exit size shown on Figure 2 represents the size attainable if the flow is expanded to Mach 6. Allowance for tunnel boundary-layer displacement thickness is included. The facility is designed with a Mach 6 nozzle but with Mach 7 energy duplication since the bow shock from a vehicle flying at Mach 7 would typically reduce the local flow Mach number to about 6 just ahead of the scramjet inlet. The effective size of the nozzle exit can be

increased to some extent by a cold shroud flow technique, described later in the report, but Figure 2 indicates the severe power limitations on facility size and altitude simulation for a 2220° K airstream.

The effect of tunnel stagnation temperature and pressure on the dynamic pressure, q , duplicated in the facility is shown in Figure 3. The solid lines denote the dynamic pressure of the flow entering the engine and the dashed lines show corresponding equivalent values which would exist ahead of the vehicle bow shock assuming the shock strength to be that required to reduce the Mach number from 7 to 6. At present, the facility is undergoing shakedown tests and operation has been confined to 30 atm stagnation pressure, where the equivalent flight dynamic pressure is from 450 to 500 psf. Typical flight operating q -values are from 500 to 1500 psf so the tunnel duplicates only those in the low range. This limitation, of course, represents a design compromise between maximizing q -value and maximizing tunnel size for a given amount of power available. Low q , or high altitude, represents the more difficult engine operating conditions aerodynamically, so testing at these conditions provides a critical assessment of engine performance.

Scramjet Ignition and Reaction Length Considerations

At high-altitude conditions, one concern is the ignition and reaction time of the fuel which, in turn, influences scramjet combustor length. Generally, the length for complete reaction is a function of the rate of mixing of hydrogen and air and chemical reaction rates are sufficiently fast that they have only a small effect on combustor length. That is, combustion is diffusion controlled and mixing dominates the criterion for scramjet combustor length. The subscale engine tests will not only be at a low q -value but the scale is about one-third to one-half that of an aircraft engine sized for a research airplane so minimizing ignition delay and reaction length is especially important for proper interpretation of results. Mixing length of fuel and air should scale, however, if combustion rate were dominated by chemical reaction time it would not scale.

Empirical formulae are available¹⁰ for estimating ignition delay time, however, the problem with trying to assess its importance on combustor length in the present geometry involves a complex, three-dimensional flow situation. The local velocities for the transverse injection case (behind a step) are influenced by wakes, vortices, boundary layers, and shocks in the combustor entrance region and are not amenable to accurate prediction.

A precedent exists for successful tests of a subscale scramjet engine with a circular cross-section configuration (9-in. diam),¹¹ so there is a strong basis for expecting that the ignition delay problem will not override other considerations and that the data can be properly interpreted. For example, the measure of the heat release along the scramjet model is a major objective of the tests and interpretation of these results can signify the importance of ignition delay.

Facility Components

An existing electric-arc-heater facility, formerly used for entry-oriented research was modified to conduct tests on the hydrogen-burning scramjet model. Existing equipment being used consists of high-pressure air storage (5000 psi), 20-megawatt dc power supply, high-pressure water cooling, test cabin and model injection apparatus, diffuser, aftercooler, 100-ft-diam vacuum sphere, control instrumentation, and magnetic tape data read-out system. New equipment required for the modification included an arc heater and plenum chamber, nozzle, hydrogen system for model fuel, steam ejector for evacuating sphere, and modification to air controls. A photograph of the arc heater, nozzle, and test cabin is shown in Figure 4.

Arc Heater and Plenum Chamber

The commercially available Huels type arc heater, Figure 5, was designed to operate at pressures up to 40 atm. Compatibility with the existing power supply was a large factor in selection of this heater. The existing power supply with silicon diode rectifiers is rated for 8000 volts to ground. The heater is operated with one electrode typically as high as 6000 volts above ground and the other electrode as much as 6000 volts below ground. Design performance at the heater exit (before mixing) is 30 atm stagnation pressure and an enthalpy level of 10 megajoules/kg (4300 Btu/lb) with 0.726 kg/sec (1.6 lb/sec) through the heater.

Just downstream of the heater is a plenum chamber where the arc-heated air is mixed with 1.542 kg/sec (3.4 lb/sec) of unheated air. This mixing concept provides a high mass flow and still allows the arc heater to operate at the higher temperatures for which operating experience exists. The design objective of the mixing chamber is to produce a flow at the exit of the chamber (nozzle throat entrance) with a uniform pressure and temperature but with minimum heat loss to the walls. The plenum chamber, designed by Linde Division of Union Carbide Corp., was patterned after a short mixing chamber for which successful tests had been made.¹²

The upstream end of the mixing chamber, Figure 5, consists of three rings, forming a divergent conical section. On both upstream and downstream faces of the middle ring are 12 sonic jets each, which direct the unheated air radially toward the center where it mixes with axially directed, arc-heated flow. Electrical insulation between the three rings insulates the arc-heater electrode from the tunnel nozzle.

Nozzle and Test Cabin

The facility nozzle, Figure 6, has a peripheral, unheated supersonic flow around three sides of the arc-heated Mach 6 flow. This unheated flow forms a 0.133-meter (5.25-in.) thick flow at Mach number 3.6 on the bottom and two sides of the hot Mach 6 flow which opens the nozzle exit size to 0.40 by 0.44 meter (15.75 by 17.25 in.). The stagnation pressure of the peripheral unheated flow is adjusted so that the static pressure at the nozzle exit matches that of the high-temperature, Mach 6 flow. This operational technique minimizes the disturbance originating at the junction of the hot and cold flow boundaries. Except for relatively large downstream cowl

locations on the engine model, this disturbance should not enter the engine. Because of the parallel exterior sidewalls of the engine, nonuniformities in the flow that do not enter the engine inlet will not affect drag and thrust measurements. The peripheral unheated supersonic flow serves three purposes, (1) allows somewhat larger model size, (2) dilutes any unburned hydrogen that might exhaust from the engine model so that there is no danger of combustion in the tunnel diffuser ducting, and (3) eliminates downstream tunnel wall cooling problems.

The insert in the upper left of Figure 6 illustrates how nozzle extension plates will be added to minimize the drag from stray eddy currents that might impinge on struts, instrumentation leads, and hydrogen lines that extend above the upper model surface. Forces arising from this effect should be small but will be investigated early in the engine test series to determine the need for the upper surface nozzle extension. Since the test cabin static pressure will generally be higher than nozzle exit pressure, the need for sealing the gap between the upper surface leading edge of the model and the tunnel nozzle upper surface will be investigated in early engine model tests. This gap sealing can be accomplished with minimum tare load on the axial force balance by either a spring-loaded plate or a plastic or rubber shield.

Hydrogen System and Vacuum Sphere

Gaseous hydrogen for model fuel is piped through 0.0063-meter (1/4-in.) diameter tubing from remotely located trailers to a high-pressure vessel on the roof of the building directly above the facility. This vessel, when pressurized to 136 atm, contains 9.07 Kgm (20 lb) of hydrogen, which is enough hydrogen for two or three tests, after which it is recharged from the trailers. The hydrogen flow control valves, also located on the roof, are remotely operated in the facility control room. Safety features incorporated in the facility include no joints in the hydrogen line between the roof and its entry into the test cabin, a ventilation hatch in the roof above the test cabin, two hydrogen detectors in the test room, and one detector in the vacuum sphere into which the tunnel exhausts.

Hydrogen flow to the model is 0.059 Kgm/sec (0.13 lb/sec) at $\phi = 2$. Airflow through the tunnel is approximately 9.07 Kgm/sec (20 lb/sec). In spite of the relatively low hydrogen flow rate, there was concern for the safety aspects of unburned hydrogen exhausting into the 30.5-meter (100 ft) diam vacuum sphere. Convincing evidence of the safety of this feature is shown in Figure 7 and illustrates one advantage of the large sphere size. If the entire 9.07 Kgm (20 lb) of hydrogen from the pressure vessel on the roof is exhausted into the sphere when it is completely evacuated, it would raise the pressure only by the small amount shown on Figure 7 at the extreme left where the concentration is 100%. Adding air to the sphere raises the pressure and decreases hydrogen concentration. In the concentration range where burning can occur, the pressure rise due to burning is shown by the cross-hatched area on Figure 7. Figure 7 shows that pressures in the sphere cannot exceed 0.4 atm even with combustion of the entire contents of the hydrogen in the pressure vessel on the roof. No condition is foreseen where the entire 9.07 Kgm (20 lb) of hydrogen

will find its way into the sphere, but the calculations for this extreme case illustrate the lack of any hazardous condition arising from hydrogen in the sphere.

Detonations in the sphere could cause much higher pressures than shown on Figure 7, however, detonations from a spark source cannot be made to occur in a spherical geometry for hydrogen-air mixtures.¹³ For the case of hydrogen-oxygen mixtures, the experiments of Reference 13 indicate that the effect of nitrogen dilution of a hydrogen-oxygen mixture is to decrease its limits of detonability so that if more than 40% nitrogen (by volume) is present in the hydrogen-oxygen-nitrogen mixture, then detonation will not occur. These experiments were conducted at 1 atm by use of balloons, but similar effects should result at the reduced pressures in the 30.5-meter (100-ft) diam vacuum sphere.

Arc-Heater Performance and Operating Problems

Although the arc heater selected for the scramjet test facility is a design that has been extensively developed and successfully used in a number of applications, there have been operating problems while attempting to make the facility fully operational. Every arc heater when coupled with a particular power supply has some unique characteristics. Initial tests with the heater were reasonably successful except that at the end of each run, the O-ring at the downstream end of the downstream electrode failed, Figures 5 and 8. Apparently, the hot tip of the electrode was dragged back across to the O-ring when the electrode contracted after its thermal expansion during the run. This could have been tolerated, except that in later runs an excessively long arc created more severe problems. In one run, the arc fired all the way to the nozzle throat section gouging a large indentation. Increasing the current in the downstream coil from 700 to 850 amps in order to strengthen the magnetic field, which causes the end of the arc to rotate and tends to block the arc from its excessively long excursions, did not cure the problem. Therefore another solution to the problem appeared necessary.

The cause of the situation which sometimes produces a good run and sometimes an excessively long arc is believed to be the lack of good electrical contact between the housing in the region of the problem O-ring and the downstream tip of the electrode, Figure 8. If this contact is good, then the major portion of the current flows into the downstream tip of the electrode, along the electrode in the upstream direction, through the arc termination region and up the center of the tube through the long arc. There are no adjacent parallel current paths in this desirable situation. On the other hand, if the electrical contact is poor at the downstream tip of the electrode, then the major portion of the current flows along the electrode from the upstream to the downstream direction, across the arc termination region, and back up the center of the tube along the arc. This produces two adjacent parallel paths of current with the flow in opposite directions and is analogous to the effect produced when an arc is struck between two rails. In this case, the concentration of the self-induced magnetic field intensity between the rails causes a curvature of the arc and pushes the arc along the rails. In the actual arc-heater configuration, the tubular electrode might be considered as one rail and the

long arc column, located along the center of the tube might be considered as the other rail. For the large currents (~ 2000 amps) carried by the arc and the electrode, the force driving the arc can be large.

In order to avoid the extra force tending to lengthen the arc due to parallel current paths, the downstream region of the heater was modified to assure a path for the electrical current in the upstream direction. Eight small pieces of flat braided cable, as used for ground wiring, were fastened to the front housing and soft soldered to the exterior surface of the downstream electrode about 0.07 meter from the end. These flat braided cables were sufficiently flexible to withstand the thermal expansion and contraction of the electrode. The cables are immersed in the water passage, but experience so far has indicated no appreciable decrease in cooling flow rate and no hot spots. The heater is presently performing satisfactorily but more operating experience is needed to conclude if the modification which eliminates the parallel current paths has cured all arc-heater operating problems. Since the modification, the O-ring has survived each time but test durations have been limited to about 10 sec. Improvement in the steadiness of the flow through the heater has been another benefit of the modification to the heater. Figure 9 shows the time histories of the arc voltage, arc current, stagnation pressure, and total enthalpy of the flow entering the throat. Solid curves are for an early run before modifying the heater, and dashed curves are data obtained from a run after the modification. These data were recorded on a magnetic tape and printed every 0.2 sec. The dashed curves are noticeably smoother; in fact, the enthalpy curve before modification is so irregular that its accuracy is doubtful, whereas the enthalpy curve after modification is smoother and more accurate. According to the bulk enthalpy measurements shown on Figure 9, which were determined from measurement of input power and heat loss to the cooling water, the enthalpy entering the throat is very close to the desired value of 2.55 megajoules/Kg (1100 Btu/lb) for the data obtained after modifying the heater. Planned additional tests will include measurements in the test flow of stagnation-point heating from which enthalpy profiles will be inferred.

Test Flow

Nozzle Design

Much of the analysis related to the design of the nozzle for the facility and to the downstream extent of mixing between the hot and cold flow has been previously reported.¹⁴ The two-dimensional Mach 6 nozzle was designed using the method of characteristics theory.¹⁵ Although chemistry effects are minor for the relatively low stagnation temperature, 2220° K, the analysis considered frozen chemistry. This is a reasonable assumption since quasi-one-dimensional calculations have shown that the chemical composition of air is essentially frozen very early in the nozzle expansion.¹⁶ Solutions of nonsimilar laminar and turbulent boundary-layer equations including multicomponent reacting gases and transverse curvature effects were used in the boundary-layer flow analysis. The system of equations describing the boundary-layer analysis¹⁷ and the corresponding FORTRAN program¹⁸ assume local

chemical equilibrium conditions. The pressure distributions along the nozzle calculated from Reference 15 were used as input in the boundary-layer analysis. Displacement thickness was calculated and the nozzle ordinates increased to allow for displacement thickness. Boundary-layer transition from laminar to turbulent flow was assumed to occur at a value of Re_{θ} of 600. This occurs just downstream of the throat where there is a steep gradient in Re_{θ} with downstream distance. Consequently, the boundary-layer analysis should be insensitive to the value of Re_{θ} chosen even if it were two to three times higher.

Flow Measurements

To date the only flow measurements which have been made are a few preliminary pitot profiles, Figure 10. The measurements shown in Figure 10 were made during shakedown testing of the arc heater and do not represent exact design operating conditions. For the data shown in this figure, the static pressures of the hot inner flow and the unheated peripheral flow were not matched. The exit pressures being unmatched should not affect profiles of the hot flow just downstream of the exit; results of Figure 10 (circular symbols) show this to be true since the profile is relatively flat. The Mach number as determined from P_{T2}/P_T is slightly higher than the design value of 6. As indicated by the maximum pressure on the flat portion of the experimental and theoretical curves on Figure 10, the test Mach number is 6.2. The theory curve represents a prediction of pressures through the boundary layer using the method of Reference 18. Also, the pitot measurements in the profile, although limited for good boundary-layer analysis, indicate that the tunnel boundary layer is thinner than predicted which would tend to account for the higher Mach number.

The square symbols in Figure 10 show the pitot profile 0.33 meter downstream of the nozzle exit and the effect of the mismatch in static pressure between the hot and the unheated flow is evident. There is a high pitot pressure value at $y = 0.23$ meter that indicates a disturbance presumably originating at the junction of the hot and unheated flows. Since the static pressure of the peripheral flow was not matched to the hot flow, this disturbance should be expected.

Some of the experimental downstream pitot profiles have shown a disturbance originating at the top of the hot flow nozzle which is caused by too high an ambient pressure in the test cabin. Figure 10 does not show this disturbance, possibly because the pitot tube spacing is too large in the region near the top of the nozzle. In any case, this disturbance will be eliminated by the use of a seal between the leading edge of the upper surface of the engine model and the top surface of the nozzle exit (see Fig. 6).

The calibration of the flow is obviously incomplete at this time. A water-cooled rake for measuring stagnation-point heating at the same locations for which pitot measurements are being made will be used to infer the local enthalpy profile in the stream. Also, gas samples of the flow will be collected and analyzed in order to determine the NO concentration in the stream. Previous arc-heater experience has shown typical NO concentration of

2% to 3%. Finally, a wedge duplicating one engine sidewall has been constructed and instrumented with a row of heat-transfer gages in order to determine where boundary-layer transition occurs. Fully turbulent flow is required at the combustor entrance region of the model because of shock-boundary-layer interaction phenomena and the wedge tests will determine if roughness strips are needed and allow experimentation with roughness strips. Since Re_{θ} is predicted to be about 1000 at the inlet exit location of the model, fully turbulent flow might be realized without roughness strips.

Engine Boundary-Layer Ingestion

The engine model in the facility ingests the boundary layer from along the top contoured surface of the hot flow nozzle. On a flight vehicle, an integrated scramjet will ingest the boundary layer from the undersurface of the fuselage ahead of the engine. These two boundary layers will generally not be identical so some exploratory calculations have been made to assess the type and magnitude of the effect that might result from lack of perfect simulation of the boundary-layer ingestion phenomenon. The exploratory calculations of the tunnel and flight vehicle boundary layers are not exactly comparable but are sufficiently close to the same flight conditions that their comparison is informative.

The boundary-layer calculations for the flight vehicle were for one of the forebody contours being considered for the X24C research airplane, Figure 11. The calculated inviscid pressure distribution, along the center-line forebody surface of this vehicle was used to calculate a two-dimensional boundary layer using the program of Reference 18. Velocity profiles and ρU profiles of the tunnel and flight vehicle boundary layers are shown in Figure 11. The flight vehicle boundary-layer profile is for a station 8.89 meters (350 in.) from the nose, which is in the neighborhood of the expected engine inlet location. The flight condition for the vehicle boundary layer corresponds to the X24C airplane flying at $\alpha = 7^\circ$ at Mach number 7.8. The static pressures in the region of the inlet for the flight vehicle are about 0.0137 atm (29 psf) and local Mach numbers in this region are about 6.3. For the tunnel, the calculations are based on a Mach number at the nozzle exit (engine inlet location) of 6 and a stream static pressure of 0.0146 atm (31 psf). The boundary-layer profiles shown in Figure 11 are thus for approximately similar conditions. The vertical distance from the surface, y/h_c , is nondimensionalized by the engine capture height. The value of h_c used for the tunnel boundary-layer calculations was 0.203 meter (8 in.) and the value for the X24C vehicle used in the calculations was 0.457 meter (18 in.). This latter value is only a tentative number since the size of scramjet engine that might be used on this vehicle is not presently finalized. In any case, Figure 11 shows that the tunnel boundary-layer displacement thickness is considerably thinner in proportion to the engine height than a flight vehicle boundary layer. The parameter, δ^*/h_c , is approximately one-half that which might be realized on a flight vehicle. Considered another way, the proportion of tunnel boundary-layer displacement to capture height would be such as to approximately simulate a 0.914-meter (36-in.) high engine on a flight vehicle. The large difference in δ^*/h_c is due principally to the difference in

the variation of ρU through the boundary layer in the two cases. In terms of the ratio of total thickness to engine capture height, the tunnel and flight boundary layers are approximately equal.

The low values of $\frac{\rho U}{\rho_\infty U_\infty}$ for the X24C boundary layer, and only moderately higher values of $\frac{U}{U_\infty}$ indicate that the momentum, ρU^2 , in the X24C boundary layer for this particular forward fuselage shape is lower than the momentum in the tunnel boundary layer. This implies a nonconservative test since a scramjet might encounter boundary-layer separation problems in flight and not in the tunnel.

The X24C forebody shape chosen for this comparison is not finalized and the ρU distribution through the boundary layer is highly sensitive to the forebody shape, so the preceding comparison should be considered as only a preliminary assessment of the simulation capability of the tunnel regarding the boundary-layer ingestion problem. It will be shown in a later section of this report that boundary-layer ingestion has only a minor effect on engine thrust.

Subscale Scramjet Model

The subscale scramjet model which will undergo the first series of tests in the facility is completed and is shown in Figure 12. The 0.203-meter-high model is about one-third to one-half the scale of an engine that might be used on a research aircraft. The scramjet model is instrumented to measure pressures, temperatures, heating rates, and engine thrust. It is also designed to allow substitution of components which vary the internal shape.

Since the model was intended to be primarily heat sink, it is constructed of copper with water cooling only in critical locations. The model design allows up to 30 seconds of testing with hydrogen burning. To conserve test times, the model will be injected into the test stream after the tunnel has reached its equilibrium condition.

The scramjet model was first conceived to incorporate water cooling only at the various leading edges. However, thermal analysis of various engine components indicated that the temperature gradients in the combustor entrance region were severe. These analyses consisted of calculating the heating rates to all internal surfaces of the engine using the integral boundary-layer technique of Reference 19. Next, computer thermal models of various engine sections were constructed using the method of Reference 20, which involves a 2-D transient finite-difference heat-transfer technique. The surface temperature distribution from this analysis is shown for the uncooled scramjet sidewall by the dashed line in Figure 13. The thermal gradients near the leading edge and in the combustor entrance region are severe and estimated thermal strains indicated that the yield point of the copper was exceeded. Since the number of tests that the uncooled model would survive could not be readily estimated for the copper in the plastic strain region, the decision was made to incorporate water cooling into selected locations. This produced a more linear calculated wall temperature distribution for a 30-sec test as shown by the solid line in Figure 13. For this more linear temperature distribution, thermal strains are greatly reduced, and the

copper model was built with cooling channels located and sized in accordance with the theoretical model that produced this improved temperature distribution.

The 0.00076-meter (30-mil) diameter leading edges of the engine sidewalls, cowl, and struts were recognized as a critical location requiring water cooling. Consequently, experimental research and analysis of the leading-edge fabrication and survival problem was undertaken and results are reported in Reference 21. The configuration with the copper tube brazed into the assembly, as shown in Figure 13, survived a higher heating in a low supersonic Mach number, combustion-heated test flow than the leading edges will encounter in the Scramjet Test Facility. The 0.00076-meter (30-mil) leading-edge diameter is one-half the diameter of the leading edges which were used on the flight-weight regeneratively cooled, leading edges of the Hypersonic Research Engine project,⁹ so the leading edges are scaled to a practical size of a flight-weight structure.

Fuel Injection Struts

The fuel injection struts proved to be one of the more difficult design problems on the subscale scramjet model and will also be a challenging design problem on a larger flight-weight engine. The minimum size strut that can be built which retains the desired aerodynamic, propulsion, and structural features will determine the minimum size engine required for meaningful tests of a flight-weight engine.

The fuel injection struts for the subscale scramjet model are constructed from OFHC copper and contain both water cooling passages and hydrogen-fuel manifolds. The hydrogen manifold cross-sectional areas are designed so that the hydrogen flow Mach number does not exceed 0.2 in order to avoid excessive losses in hydrogen total pressure.

The struts are designed to inject hydrogen over a fuel equivalence ratio range from 0.5 to 2.0. To insure fuel choking at the injection orifices, q_f/q_a was chosen to be 0.6 at the lowest fuel equivalence ratio of 0.5. This fixed the hydrogen-fuel manifold pressures in a range from 3.843 to 15.374 atm (56.5 to 226 psia) for the flow conditions in the Scramjet Test Facility. Orifice spacing, and therefore the number of orifices along the struts was calculated by using a value of 3.125 for the ratio of orifice spacing to effective gap width, where effective gap width is one-half the distance between struts and the spacing is determined in a plane normal to the flow direction. The selection of the 3.125 value was based on experimental results and this spacing should allow adequate fuel penetration and lateral mixing. To determine the required fuel mass flow rate for each orifice, the air passages to be fueled were assumed to be divided into equal areas (except near the top surface and the cowl) surrounding each orifice and the air mass flow rate in each of these areas was computed using local mass flow rate distributions from inlet tests.⁶ Next, the hydrogen temperature at each orifice was calculated and an orifice discharge coefficient was assumed. Thus, with the hydrogen mass flow rate, total temperature, total pressure, and orifice discharge coefficient available for each orifice, the geometric orifice diameters were calculated. The

average orifice diameter was about 0.043 inch with smaller orifices near the top surface and larger ones near the cowl. In initial tests, however, those orifices near the cowl will be undersized to guard against thermal choking in this area of high heating.

Instrumentation

Measurements to be made during a test include drag or thrust, heat transfer, pressures, and wall temperature at selected locations. Data recording capability exists for 200 channels of model instrumentation in addition to another 49-channel magnetic tape system for recording measurements of tunnel parameters. The one-component force balance is designed for a maximum load of 200 pounds. Measurement of drag or thrust will be attempted at the same time heat transfer and pressures are being measured if the tare loads due to the many instrumentation leads can be sufficiently minimized. If these tare loads are too large, then the other instrumentation loads will be disconnected for the tests made with the force balance.

The balance measures internal drag or thrust since the external surfaces of the model are flat and parallel to the drag axis. Consequently, with the exception of a few beveled surfaces, pressures acting on model exterior surfaces will not affect drag and thrust measurements. On a flight vehicle, engine modules will be adjacent to each other and in order to simulate the adjacent engine (3-D effects), the tunnel model was designed with an exterior bevel at the leading edge of the sidewalls, Figure 14. The exterior bevel is at the same angle as the interior surface, 5.6°, and extends 0.1369 meter (5.39 in.) streamwise. Some pressures on the beveled surface will be measured, but their contribution to the drag, which is expected to be measured at $\phi = 1$, is only 4.3% so forces on the bevel can be readily calculated to sufficient accuracy. Skin friction on the exterior model surfaces can also be readily estimated with sufficient accuracy. At the $\phi = 1$ test condition, skin friction on the exterior surface is estimated to be about 3.4% of the total drag.

Heat-transfer gages, pressure orifices, and thermocouples are located throughout the interior surface of the model, Figure 14. This instrumentation is generally arranged along lines parallel to the cowl surface and along oblique lines parallel to the sweepback sidewall leading edges. Heating rate to the model surface will be measured using Gardon-type gages. These gages have a 0.0001-meter (0.004-in.) thick constantan foil and chromel wires at the center and at the edge of the foil. The foil portion is 0.0023 meter (0.090 in.) diam, mounted on a 0.0047-meter (0.1875 in.) o.d. copper tube so that the foil is flush with the model surface. The gages are calibrated under a radiant heat source and the difference in temperature between the center and the edge of the constantan foil is proportional to the heating rate. With this type of gage, there is an uncertainty when measuring convective heating, because of the aerodynamic effect of the local hot spot in the center of the gage. This hot spot effect is much more severe in laminar than in turbulent flow. However, following the technique described in Reference 22 to determine the size of any correction for the local hot spot, the magnitude of the correction is estimated to be less than 5%.

On the engine inlet surfaces where the boundary layer is laminar, surface temperatures are not high, thus the temperature difference between center and edge of the gage is small, and in the combustor region where there is a large temperature difference, the boundary layer is turbulent. Although the technique of Reference 22 predicts a rather small effect for this particular gage design under the heating conditions expected in the engine model, this hot spot effect on heat-transfer measurement needs further experimental research. In any case, this particular type of gage seems suited to these tests and will give a fast response (95% of gage output in less than 1 sec). This feature permits a relatively short test duration or opens the possibility of varying ϕ during a test.

Pressure orifices on the engine model are 0.00165 meter (0.065 in.) diam and lag time is estimated to be less than 6 seconds. Pressure measurements are the critical parameter which determines the required test duration. The circular symbols in Figure 14 show locations on the model where pressures are measured.

In addition to the temperature measurements determined by the heat-transfer gages (temperatures at the edge of the gage are one of the outputs of the gage), there are a number of thermocouples distributed throughout the model as shown by the diamond symbols in Figure 14. With the temperature sensor coverage shown, a reasonably well defined wall temperature history can be obtained for use in monitoring for local hot spots and for interpreting heat-transfer results.

Predicted Performance

Estimates of the performance of the scramjet model have been made in order to size the force balance and to determine how well the engine is performing during tests. A cycle analysis has been performed for the three-dimensional scramjet engine model using a computer program developed for the computation of the performance of hydrogen-fueled supersonic combustion ramjet engines. The cycle process and performance parameters are based on a one-dimensional fluid dynamic model and real-gas equilibrium thermodynamic properties. A schematic of the one-dimensional flow model and the control volume used in the engine analysis are shown in Figure 15. The change in engine flow parameters through the engine are computed one-dimensionally. The one-dimensional flow model includes the ability to account individually and separately for heat removal (because of surface heat transfer) from the flow entering the engine (forebody heat transfer) and from the flow as it passes through the inlet, combustor, and nozzle. The one-dimensional flow model also includes the effects on engine performance of boundary-layer losses to the flow entering the inlet, of flow spillage through the bottom of the inlet (additive drag), of injected fuel temperature, and of plume drag. Through application of the control volume concept to the control volume of Figure 15 the internal thrust of the engine (relative to the inlet entrance) can be expressed by the following relation.

$$\text{Internal thrust} = (\text{Mom})_{\text{NE}} - (\text{Mom})_{\text{IE}} - F_{x, \text{plume}} - \frac{P_1 + P_2}{2} (A_{\text{cowl}} - A_1) \quad (1)$$

In the estimates of the performance for the scramjet model, the terms $(\text{Mom})_{\text{NE}}$, $(\text{Mom})_{\text{IE}}$, and F_x , plume are nozzle exit flow momentum, inlet capture flow momentum, and plume drag all in a direction parallel to the cowl. The last term of Equation (1) is the approximation for the additive drag used in the scramjet performance calculations (subscripts refer to Fig. 15), and this term is a function of the amount of spillage.

The estimates of the thrust of the scramjet model as presented in Figures 15 include an estimate for the additive drag but do not include an estimate for the plume drag. Estimates indicate that the plume drag reduces the thrust by as much as 14% for $\phi_{\text{fuel}} = 1.0$ and A_4/A_1 of 3.5. Since the wind-tunnel model is not regeneratively cooled, the heat loss to the walls was approximated using the method of Reference 19 and the thrust penalty due to this predicted heat loss evaluated. From these performance predictions and those of Reference 11, the penalty to engine thrust imposed by the engine flow heat loss not being added back into the fuel is about 8%. The results of the performance calculations indicate there is a strong effect of fuel equivalence ratio on thrust produced, Figure 15(a), and a strong effect of increasing nozzle exit area, Figure 15(b). At $\phi = 1.0$, with the nozzle exit area equal to the cowl area and the nozzle exit flow parallel to the cowl ($\beta = 0$), the expected thrust of the model is about 90 pounds. A technique has been devised for modifying the model to permit tests with larger nozzle exit areas but these tests will be conducted later in the program.

The nonuniformity of the tunnel flow ingested by the model is illustrated in Figure 16 by the theoretical and experimental Mach number distributions across the scramjet model capture height in the tunnel nozzle exit plane. The Mach number values shown by the circular symbols were determined from ratios of pitot pressure measurements and measured wall static pressure. Agreement with the predicted stream profile is excellent even though this ratio is not generally regarded as the best method for obtaining Mach number. These pitot data are the same as presented in Figure 10 in the form of pitot pressure to tunnel stagnation pressure ratios and the results shown on Figure 10 indicate a slightly higher Mach number than the data of Figure 16. Figure 17 indicates that the engine thrust is relatively insensitive to the average Mach number entering the inlet. The arrow on Figure 17, showing the area-weighted average Mach number entering the scramjet inlet, is determined from the data on Figure 16. The average Mach numbers for all three profiles shown on Figure 16 (measured and predicted tunnel profiles and the predicted flight vehicle profile) are almost identical and indicate that boundary-layer ingestion will have only a small effect on thrust. These results are, of course, based only on gross momentum considerations and major effects could occur if shock-boundary-layer interactions cause flow separation or some form of improper burning in the combustor.

Research Capabilities

When accurately calibrated, the Langley Scramjet Test Facility offers the potential for conducting research which can supply a better understanding of hydrogen-burning scramjet internal flow, heat transfer, and performance. The primary initial

research effort will be directed toward force, heat transfer, and pressure measurements using the existing scramjet model. Interchangeable parts on the model permit configuration changes without fabrication of an entire new model. For example, two interchangeable sets of fuel injection struts have already been constructed which will be tested in the existing model. In addition, modifications to these struts such as different fuel injection orifice sizes are planned. Other planned research effort, utilizing this facility, includes flow surveys inside the engine model and the collection of gas samples for analysis of the composition of the engine exhaust flow. This effort should lead to more detailed knowledge of combustion efficiency and engine internal flow phenomena.

The scramjet model is presently designed with flat exterior surfaces parallel to the drag axis and this limits the basic test configuration to the case where the nozzle exit area is equal to the geometric capture area. However, a technique has been devised to permit testing with a nozzle extension which increases the engine nozzle exhaust area. Figure 18 shows a cross-sectional view through the engine and the planned nozzle extension to illustrate this test concept. The exterior walls of the nozzle extension are also parallel to the engine drag axis (making them insensitive to exterior flow pressure forces) except for one forward-facing surface. This forward-facing surface is not in the flow of the main stream, however, it is connected to a one-component drag balance in order to determine the force on the plate due to eddy flows. The drag or thrust measurement on the entire engine model will be corrected for the force on the forward-facing surface. Because of the poor quality of the flow exterior to the engine, an extension of the cowl and sidewalls might be required at least part of the way toward the end of the nozzle extension. The technique will permit demonstration of significantly higher thrust (see Fig. 15(b)) and allow research on nozzle flow problems.

The facility is specifically tailored to the task of developing technology for an integratable scramjet module and is particularly suitable for this phase of the total effort. When the technology is more firmly established, future tests of larger or full-scale engines, incorporating regeneratively cooled flight-weight structures will have to be conducted in larger facilities. Suitable facilities of this type exist although they might require minor modifications. This latter type of flight-weight, complete engine testing, with fuel controls, and other flight hardware should be undertaken before actual flight tests of an engine.

References

- ¹Henry, J. R., and Anderson, G. Y., "Design Considerations for the Airframe-Integrated Scramjet," TM X-2895, Dec. 1973, NASA.
- ²Becker, John V., "New Approaches to Hypersonic Aircraft," Presented at Seventh Congress of International Council of Aeronautical Sciences, Rome, Italy, Sept. 1970.
- ³Henry, John R., and Beach, H. Lee, "Hypersonic Airbreathing Propulsion Systems," Vehicle Technology for Civil Aviation - The Seventies and Beyond, SP-292, 1971, pp. 157-177, NASA.

- ⁴Henry, John R., and McLellan, C. H., "Air-breathing Launch Vehicle for Earth-Orbit Shuttle - New Technology and Development Approach," Journal of Aircraft, Vol. 8, No. 5, May 1971, pp. 381-387.
- ⁵Beach, H. Lee, "Supersonic Mixing and Combustion of a Hydrogen Jet in a Coaxial High-Temperature Test Gas," Presented at AIAA/SAE Eighth Propulsion Joint Specialist Conference, New Orleans, La., Nov. 29-Dec. 1, 1972.
- ⁶Trexler, Carl H., and Souders, Sue W., "Design and Performance at a Local Mach Number of 6 of an Inlet for an Integrated Scramjet Concept," TN D-7944, Aug. 1975, NASA.
- ⁷Anderson, G. Y., and Cooderum, P. B., "Exploratory Tests of Two Strut Fuel Injectors for Supersonic Combustion," TN D-7581, 1974, NASA.
- ⁸Wieting, Allan R., and Guy, Robert W., "Preliminary Thermal-Structural Design and Analysis of an Airframe-Integrated Hydrogen-Cooled Scramjet," AIAA Preprint 75-137, Presented at AIAA 13th Aerospace Sciences Meeting, Pasadena, Calif., Jan. 20-22, 1975.
- ⁹Hypersonic Research Engine Project - Phase II - Air Research Rep. No. AP-72-8237, Structures and Cooling Development, Final Technical Data Report (U). Data Item 55-7.18, CR-112087, May 18, 1972, Confidential, NASA.
- ¹⁰Pergament, H. S., "A Theoretical Analysis of Nonequilibrium Hydrogen-Air Reactions in Flow Systems," Paper No. 63-113, AIAA-ASME Hypersonic Ramjet Conference, April 1963.
- ¹¹Bahr, D. W., Kenworthy, M. J., Hoelmer, W., and King, R. C., "Scramjet Exploratory Development Program," CR-1502, Prepared by General Electric Co., Cincinnati, Ohio, Feb. 1970, Confidential, NASA.
- ¹²Henson, J. R., and Simmons, C. E., "An Experimental Investigation of Mixing High Temperature Air With Ambient By-Pass Air by Upstream Injection," AEDC-TR-66-146, Nov. 1966.
- ¹³Cassult, Leon H., "Experimental Investigation of Detonation in Unconfined Caseous Hydrogen-Oxygen-Nitrogen Mixtures," ARS Journal, pp. 1122-1128, Aug. 1961.
- ¹⁴Anders, John B., Sebacher, Daniel I., and Boatright, William B., "Fluid Flow Analysis of a Hot-Core Hypersonic Wind-Tunnel Nozzle Concept," TN D-6768, May 1972, NASA.
- ¹⁵Dash, S., "The Determination of Nozzle Contours for Rotational Non-Homentropic Gas Mixtures," ATL TR-148, Advanced Technology Laboratories, Inc., Mar. 1970.
- ¹⁶Lordi, J. A., Mates, R. E., and Moselle, J. R., "Computer Program for Numerical Solution of Nonequilibrium Expansions of Reacting Gas Mixtures," Rep. No. AD-1689-A-6 (Contract No. NAS-109), Cornell Aeron. Lab., Inc., Oct. 1965.
- ¹⁷Anderson, Larry W., and Kendall, Robert N., "A Nonsimilar Solution for Multicomponent Reacting Laminar and Turbulent Boundary Layer Flows Including Transverse Curvature," AFWL-TR-69-106, U.S. Air Force, Mar. 1970 (Available from DDC as AD 867 904).
- ¹⁸Anderson, Larry W., Bartlett, Eugene P. M., and Kendall, Robert M., "User's Manual. Vol. I - Boundary Layer Integral Matrix Procedure (BLIMP)," AFWL-TR-69-114, Vol. I, U.S. Air Force, Mar. 1970.
- ¹⁹Pinckney, S. Z., "Turbulent Heat-Transfer Prediction Method for Application to Scramjet Engines," TN D-7810, Oct. 1974, NASA.
- ²⁰Garrett, L. B., and Pitts, J. I., "A General Transient Heat-Transfer Computer Program for Thermally Thick Walls," TM X-2058, Aug. 1970, NASA.
- ²¹Pinckney, S. Z., Guy, R. W., Beach, H. L., and Rogers, R. C., "Subscale Hydrogen-Burning, Airframe-Integrated-Scramjet: Experimental and Theoretical Evaluation of a Water-Cooled Strut Leading Edge," TM X-72682, May 1975, NASA.
- ²²Woodruff, L. W., Hearne, L. F., and Keliher, T. J., "Interpretation of Asymptotic Calorimeter Measurements," AIAA Journal, April 1967, pp. 795-797.

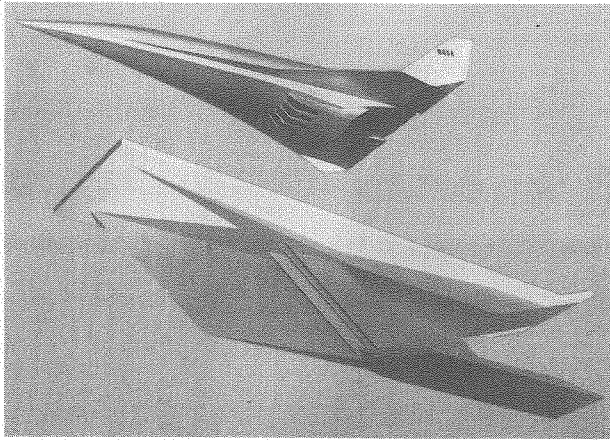


Figure 1. Airframe-integrated supersonic combustion ramjet.

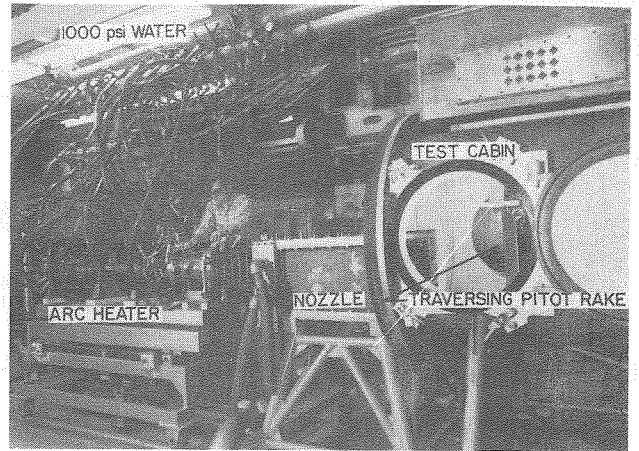


Figure 4. Photograph of Scramjet Test Facility.

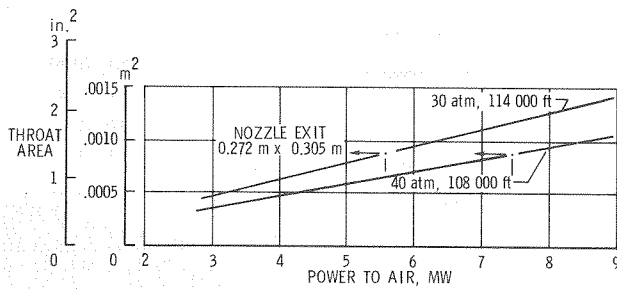


Figure 2. Power in airstream as function of tunnel size. $T_T = 2220^\circ \text{K}$.

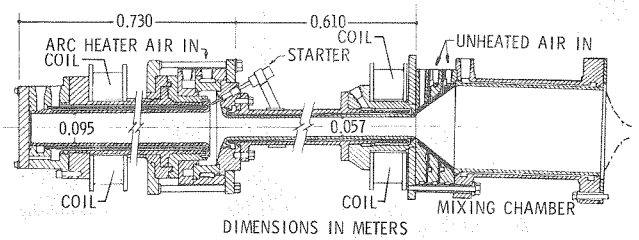


Figure 5. Cross section of arc heater and plenum chamber. (Manufactured by Linde Division of Union Carbide Corp.)

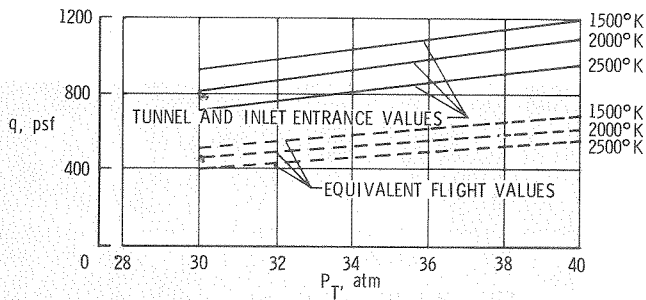


Figure 3. Attainable dynamic pressures. (Equivalent flight values assume shock ahead of inlet which reduces Mach number from 7 to 6.)

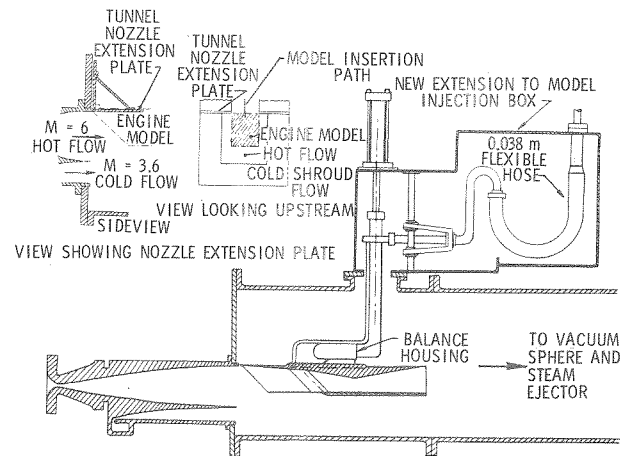


Figure 6. Sketch of test cabin and model injection modification.

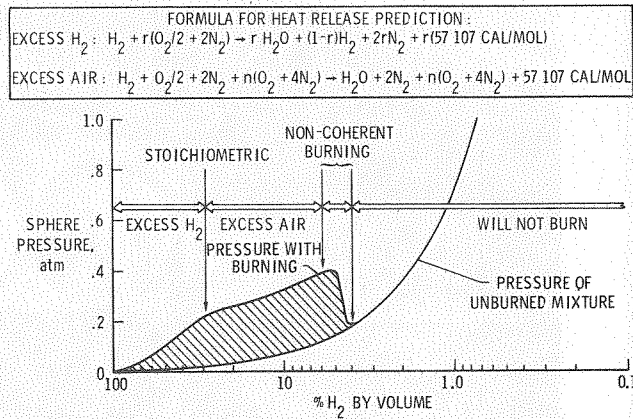


Figure 7. Maximum sphere pressures due to heat release by combustion of 20 pounds of hydrogen.

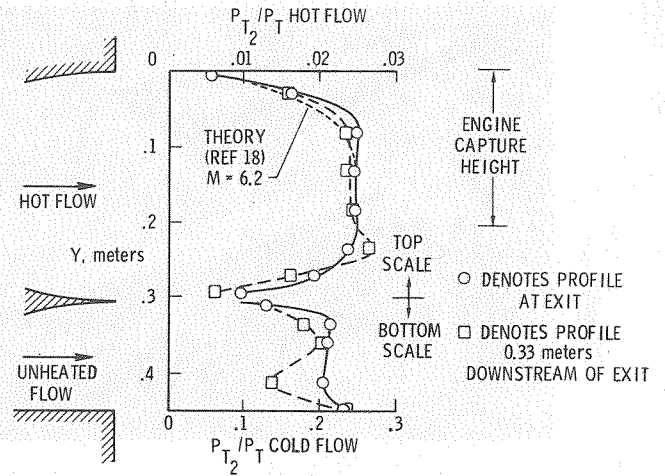


Figure 10. Pitot pressure profiles at nozzle exit and 0.33 meter downstream of exit. Preliminary test. Static pressures of hot and unheated flows were not matched.

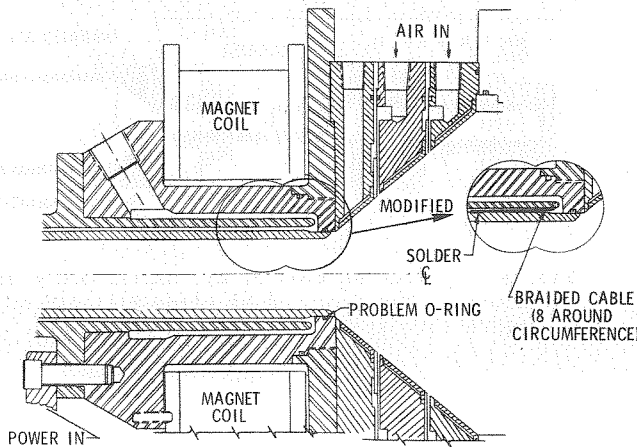


Figure 8. Enlarged view of downstream portion of arc heater.

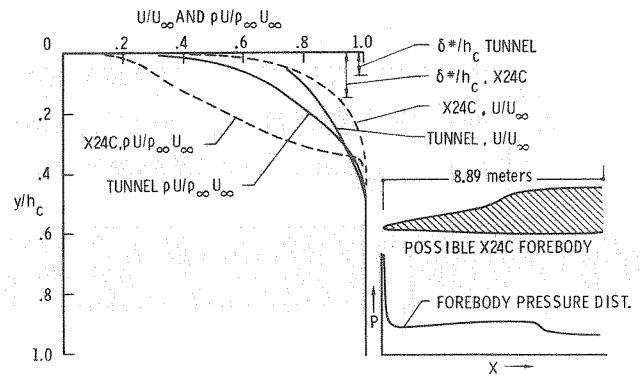


Figure 11. Theoretical boundary-layer characteristics of flight vehicle and tunnel nozzle. Capture height, h_c , of model = 0.203 meter and of flight scramjet = 0.457 meter.

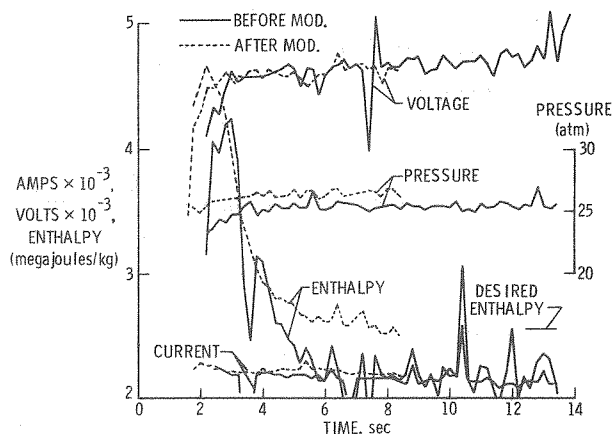


Figure 9. Time variation of arc voltage and current, and heater enthalpy and pressure.

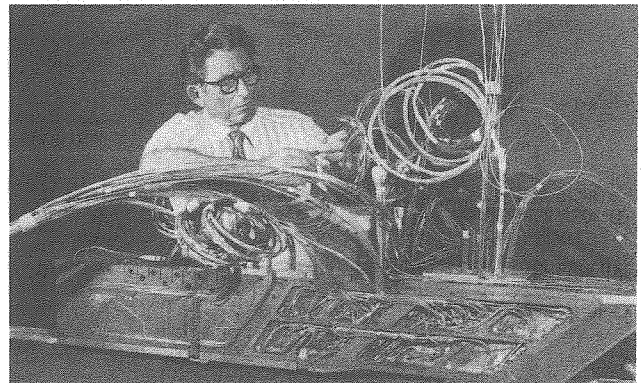


Figure 12. Photograph of partially completed hydrogen-burning scramjet model. (Exterior side plate removed.)

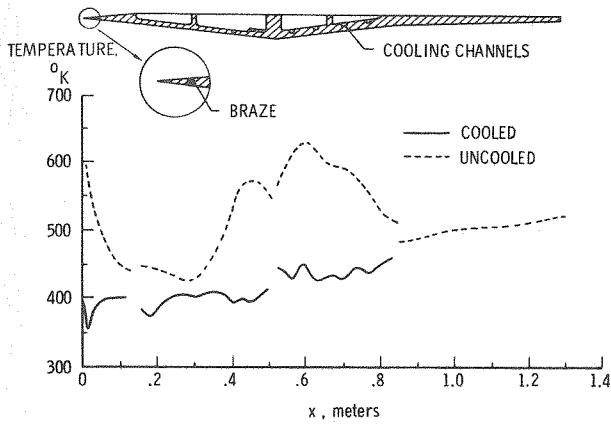


Figure 13. Predicted wall temperature for 30 sec test.

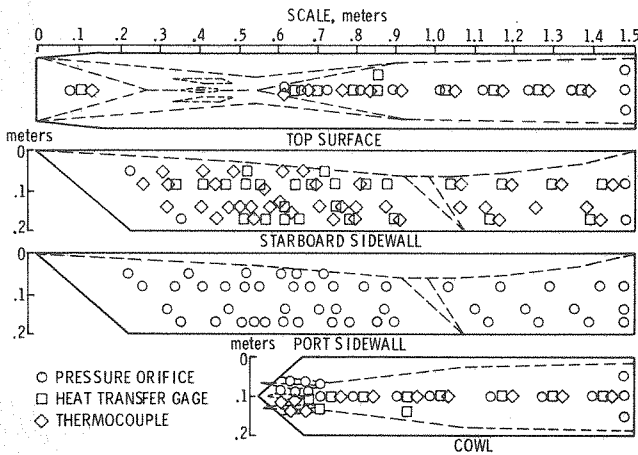


Figure 14. Location of instrumentation on scramjet engine model.

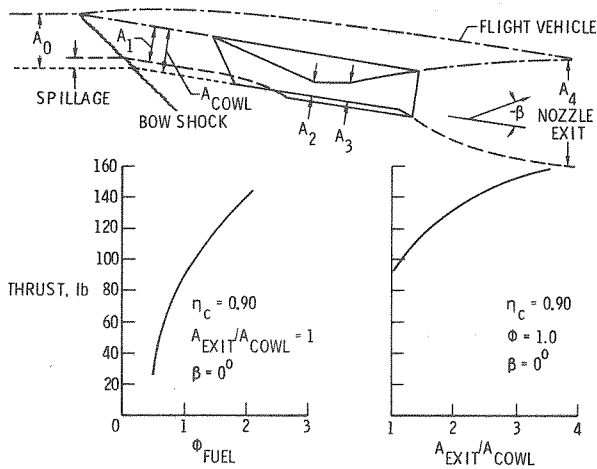


Figure 15(a) Effect of fuel equivalence ratio on engine thrust.

Figure 15(b) Effect of nozzle exit size on engine thrust.

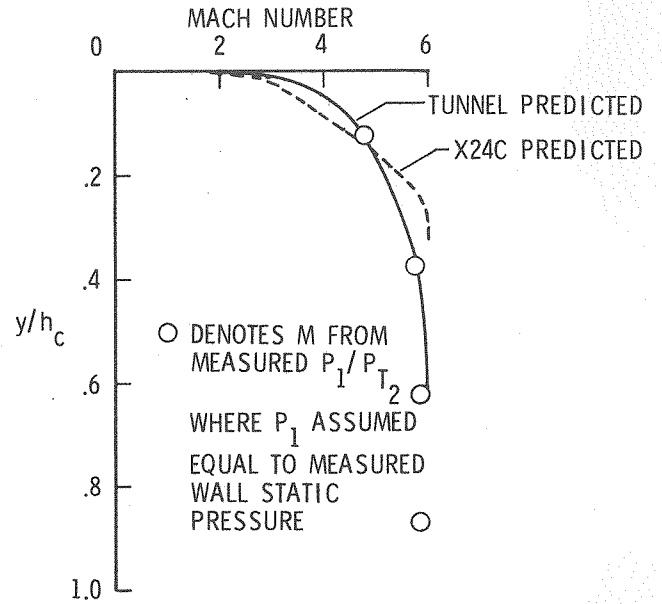


Figure 16. Mach number distribution across inlet entrance region. (h_c of model = 0.203 m, h_c of flight vehicle = 0.457 m.)

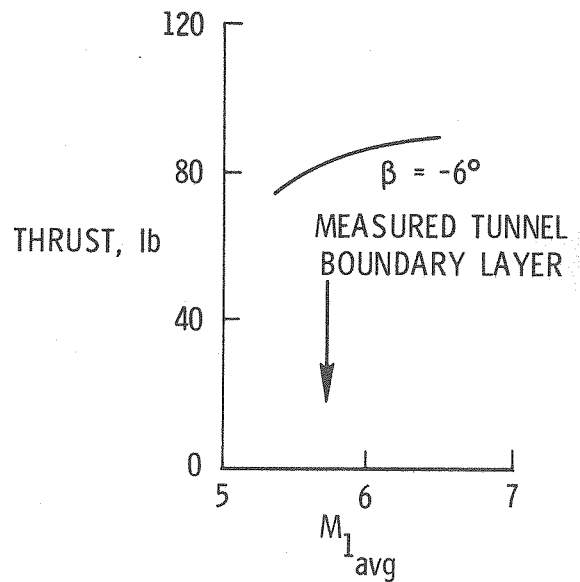


Figure 17. Effect of tunnel boundary layer on model thrust.

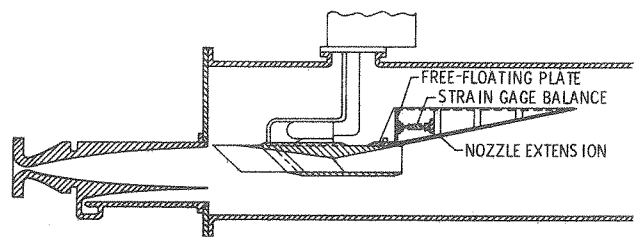


Figure 18. Concept for testing with nozzle extension bolted to rear portion of engine to evaluate engine plus nozzle internal drag and thrust.